American Mineralogist, Volume 83, pages 1045–1053, 1998

Cation sites in Al-rich $MgSiO_3$ perovskites

D. Andrault,[1,*] D.R. Neuville,[1] A.-M. Flank,[2] and Y. Wang[3]

[1]Laboratoire des Géomatériaux, IPGP, CNRS-ESA 7046, Paris 75252, France
[2]Laboratoire pour l'Utilisation du Rayonnement Electromagnétique, Orsay 91405, France
[3]CHIPR, State University of New York, Stony Brook, New York 11794, U.S.A.

Abstract

Local structure analysis of Al-containing magnesium silicate perovskite has been carried out with X-ray absorption spectra recorded at the Mg, Al, and Si *K*-edges using the SA32 beam-line of SuperAco (Orsay, France). The Al-XAFS spectrum of $(MgSi)_{0.85}Al_{0.3}O_3$ perovskite (synthesized in a multi-anvil apparatus) cannot be explained by assuming that Al^{3+} occurs in octahedral or dodecahedral sites only. This conclusion is based on comparison between Al-spectrum and those recorded at the Mg and Si *K*-edges for the same structure, general trends found for Al-spectra in various atomic sites, and ab-initio calculations using the FEFF-6 code. Thus, Al appears to be partitioned between both octahedral and dodecahedral perovskite sites. However, the structural accommodations needed to stabilize Al^{3+} cation in such different sites are not straightforward. Also, Mg *K*-edge spectra in enstatite and perovskite were compared with those previously reported at the Fe *K*-edge for the same structures, confirming that these two elements are located in the same polyhedra in both structures, and thus that Fe^{2+} enters the dodecahedra of the silicate perovskite.

Introduction

Although the first silicate perovskite synthesized in a diamond-anvil cell was prepared using pyrope as the starting material (Liu 1974), the site occupancy of Al in $MgSiO_3$ with the perovskite structure remains uncertain. $MgSiO_3$ perovskite can accommodate significant amount of Al^{3+} as pyrope ($Mg_3Al_2Si_3O_{12}$) and grossular ($Ca_3Al_2Si_3O_{12}$) were observed to transform fully into the perovskite-structure at 26.5 and 30.2 GPa, respectively (Irifune et al. 1992; Kesson et al. 1995; Yusa et al. 1995). One possibility is that two Al^{3+} cations substitute for a pair of Mg (or Ca) on the dodecahedral site and Si on the dodecahedral site in the silicate perovskite, maintaining electrical neutrality without formation of vacancies. However, the structural distortion needed to accommodate the same type of atom in both the octahedral and dodecahedral sites needs to be explained (the volume ratio in $MgSiO_3$ perovskite is about 4.3, see Andrault and Poirier 1991). This type of coupled substitution occurs along the pyrope-majorite joint, where two Al^{3+} substitute for a pair of Mg and Si in the octahedral site. The possibility of Al substitution on both perovskite sites is largely supported by recent ab-initio calculations showing that pure corundum could undergo a phase transformation to perovskite at very high pressures (Thomson et al. 1996).

The other possibility is that Al enters in only one of the two perovskite sites, more likely the octahedral site as observed in aluminous $XAlO_3$ perovskites (X^{3+} = Sc, Y, Gd . . .). In this case, either many charged vacancies should form to maintain electroneutrality (Al^{3+} substitutes for Mg^{2+} or Si^{4+} in $MgSiO_3$), or a consequent amount of Si or Mg should change coordination sites to form $(Mg_{0.85}Si_{0.15})(Al_{0.3}Si_{0.7})O_3$ or $(Mg_{0.7}Al_{0.3})(Mg_{0.15}Si_{0.85})O_3$ perovskite (A. Hofmeister, personal communication). In these cases, the volume ratio between octahedra and dodecahedra would most probably be affected, because Mg^{2+}, Al^{3+}, and Si^{4+} show significantly different ionic radii. This is in disagreement with previous reports showing that the Al_2O_3 substitution in $MgSiO_3$ occurs with reduced variation of the *Pbnm* orthorhombic distortion (see Table 1).

Obtaining quantitative information on the local structure around light elements remains an experimental challenge, especially for high-pressure minerals for which the available volume is smaller than 1 mm^3. Spectroscopic studies, using X-ray absorption (XAFS) and electron energy loss (EELS), recently addressed changes of the local structure of Si in SiO_2 polymorphs (Li et al. 1994; Henderson et al. 1995; Sharp et al. 1996). Most of the reported experimental features are located near the absorption edge, and are thus related to photoelectron multiple scattering (X-ray absorption near edge spectroscopy, XANES; energy loss near edge spectroscopy, ELNES). Various theoretical approaches have been used to reproduce the experimental spectrum of stishovite. Good agreement on the energy position of the XANES features was first obtained after comparison with the theoretical density of state (Li et al. 1994). Multiple scattering calculations were then used to improve agreement between experiments and theory, in reproducing experimental intensities (Wu et al. 1996).

* E-mail: andrault@ipgp.jussieu.fr

0003–004X/98/0910–1045$05.00

TABLE 1. Unit-cell parameters of silicate perovskites

Composition Symmetry	*$MgSiO_3$ *Pbnm*	†$Mg_3Al_2Si_3O_{12}$ *Pbnm*	‡$CaSiO_3$ *Fm3m*	§$Ca_3Al_2Si_3O_{12}$ *Pbnm*
a (Å)	4.7754	4.778	5.052	5.007
b (Å)	4.9292	4.938	5.052	5.104
c (Å)	6.8969	6.943	7.144	7.201
V (Å^3)	162.18	163.78	181.9	183.96
a/*c*	0.692	0.688	0.707	0.695
b/*c*	0.714	0.711	0.707	0.709

Note: Addition of Al produces a slight change of the orthorhombic distortion for $MgSiO_3$ or a symmetry break down for $CaSiO_3$. Both garnet-composition perovskites show a volume increase of about 1% in comparison with $MgSiO_3$ or $CaSiO_3$ phases. For $CaSiO_3$ perovskite, we report values for a quadruple cubic unit cell to facilitate comparison with other compounds.

* Ross and Hazen (1989).
† Irifune et al. (1992).
‡ Wang et al. (1989).
§ Yusa et al. (1995).

At the present time, this type of calculation (see Natoli and Benfatto 1986; Rehr et al. 1992; Cabaret et al. 1996) is only feasible if the local structure is well known. For unknown local structures, comparison between spectra recorded at the same *K*-edge for various types of known atomic sites remains a very useful fingerprinting tool, especially for light-element studies where the energy range of the XAFS spectra is limited (Ildefonse et al. 1995; Li et al. 1995). These comparisons most often provide information on the coordination number for a given element, and frequently on the site distortion.

Only a few X-ray absorption studies report a local structure analysis of perovskite-type compounds under high pressure. Most of them use XAFS in an energy dispersive mode, which provides a convenient experimental configuration to record the absorption spectra as a function of pressure in a diamond-anvil cell. This technique is the most useful when X-ray diffraction is not significant, as for example during phase transformations or in low symmetry crystals. For example, Fisher et al. (1990) described the mechanism of the cubic to tetragonal ferroelastic transformation occurring in $SrTiO_3$ at about 12 GPa. Because XAFS is very sensitive to local distortion, it also has been used to analyze the perovskite distortion with pressure (Andrault and Poirier 1991). In *Pbnm* ($SrZrO_3$ and $CaGeO_3$) perovskites, the octahedral distortion appears strongly variable with increasing pressure, confirming that the perovskite distortion is mainly controlled by the size of the polyhedra. However, these results on analogous compounds might not be directly transferable to the compression mechanism of Al-(Mg,Fe)SiO_3 perovskites relevant to the Earth. Unfortunately, collection of XAFS spectra at the Al, Mg, and Si *K*-edges at high pressure is not feasible because samples are too small, and the absorption of the diamonds is much too high at these low *K*-edge energies.

To understand better the local structure in silicate perovskite, we collected X-ray absorption spectra at the Mg, Si, and Al *K*-edges in $MgSiO_3$, $(Mg_{0.9},Fe_{0.1})SiO_3$, and $(Mg,Si)_{0.85}Al_{0.3}SiO_3$ perovskites. Comparisons were made with spectra of Mg with various coordination numbers, with Fe in octahedral or dodecahedral coordination, with Si in the octahedral sites of stishovite, as well as with calculated spectra. The high energy part of the Si *K*-edge spectra is extended sufficiently to allow a brief discussion on the extended fine structures (EXAFS). Finally, we compare this set of data with spectra obtained at the Al-*K* edge in Al-rich $MgSiO_3$ perovskite to examine the Al local structure in the perovskite.

EXPERIMENTAL METHODS

Three starting compositions were used: pure $MgSiO_3$, Fe-bearing $(Mg_{0.9},Fe_{0.1})SiO_3$, and Al-bearing $(MgSi)_{0.85}Al_{0.3}O_3$. Fine powders of synthetic enstatites or homogeneous glass (Al-bearing) were packed in rhenium or platinum capsules, and loaded in a 2000-ton uniaxial split sphere apparatus (USSA-2000). Syntheses were conducted at 26 GPa and 1973 K for 1 h. All high-pressure experiments were performed at the Center for High Pressure Research at the Stony Brook High Pressure Laboratory, State University of New York at Stony Brook. Recovered samples were checked by X-ray diffraction, and no phase other than perovskite was detected. For the Al-perovskite samples, this was achieved using an homogeneous glass as starting material only, because traces of corundum were detected in previous synthesis using a mix of $MgSiO_3$ and Al_2O_3 powders. We also examined the homogeneity of samples using electron microprobe analysis (EMPA). For the Fe-bearing perovskite, Parise et al. (1990) gave an average structural formula of $Mg_{0.880}Fe_{0.106}Si_{1.007}O_3$, which evidences low Fe^{3+} content. Samples were sectioned in order to achieve a maximum surface of around 1 mm^2 required to collect XAFS spectra at the light element *K*-edges. Cutting oil was removed from sample surfaces using acetone. Two samples of Al-bearing perovskite were synthesized to achieve an available surface area of about 2 mm^2, to compensate for the low Al-content of this compound.

Other materials used in this study are Al_2O_3 corundum (Merck), synthetic enstatite crystallized at 1350 °C (given by L. Thieblot), natural pyrope from Dora-maira, Italy (Téqui et al. 1991), natural albite from Modane, Italy (given by P. Richet), natural spinel from Norway (given by P. Bariand), and natural stishovite from Meteor Crater, Arizona (given by P. Gillet).

All samples were mounted on copper slides. Silver lacquer was used to ensure good electrical conductivity between sample and slide. X-ray absorption spectra were then collected at the SA32 beamline at the SuperAco storage ring of LURE (Orsay, France), operating at 800 MeV and with beam current between 300 and 150 mA. Double-crystal monochromators using beryl $(10\bar{1}0)$, quartz $(10\bar{1}0)$, and InSb (111) were used at the Mg, Al, and Si *K*-edges with experimental energy resolution of 0.4 eV (Mg), 0.3 eV (Al), and 0.7 eV (Si). The available energy range at the Mg and Al *K*-edges was thus limited by the monochromator composition. The X-ray beam was focused on a 500 × 200 μm^2 spot at the sample location

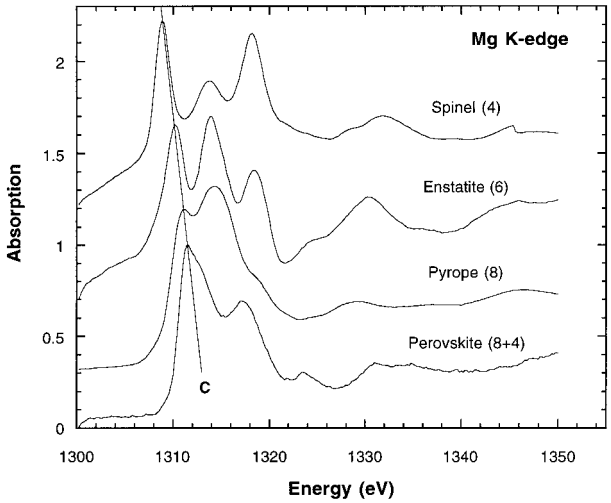

FIGURE 1. Mg *K*-edge XAFS spectra of $MgAl_2O_4$ spinel (Mg, CN = 4), $MgSiO_3$ enstatite (Mg, CN = 6), $Mg_3Al_2Si_3O_{12}$ pyrope (Mg, CN = 8), and $MgSiO_3$ perovskite (Mg, CN = 12 such that 8 of the O atoms are closer to Mg than the remaining 4). The perovskite spectrum clearly follows the trend proposed by Ildefonse et al. (1995). Significant energy shift of the first resonance occurs with increasing CN.

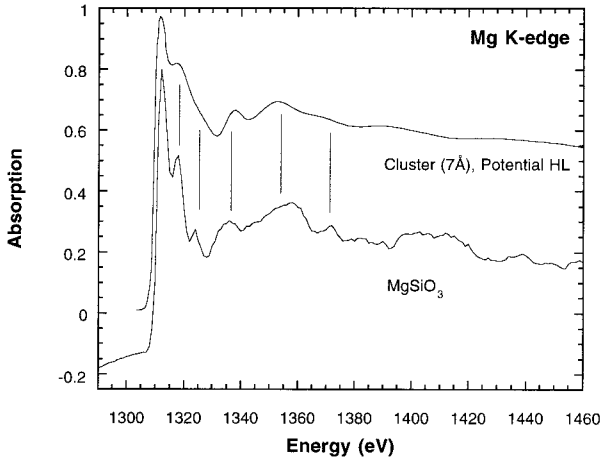

FIGURE 2. Mg *K*-edge experimental spectrum and multiple scattering calculation (FEFF-6) for $MgSiO_3$ perovskite. Cluster size and maximum path length were set to 7 Å, thus containing up to 177 atoms. Vertical lines correlate equivalent features.

using a toroidol mirror. Photo-absorption spectra were recorded by measuring total electron yield (drain current) for all samples, and X-ray fluorescence spectra were recorded at the silicon *K*-edge for $MgSiO_3$ perovskite and stishovite. Steps of 0.2 and 1 eV were used to collect XANES and EXAFS, respectively. Experimental data were recorded relatively to *K*-edges of Mg in MgO (1308.5 eV), Al in Al-foil (1559 eV), and Si in c-Si (1839 eV). At the Al *K*-edge, we also used the energy value of the peak C in corundum (1567.4 eV; see Ildefonse et al. 1998) to compare our spectra with previous ones, which is corrected by −1.3 eV from the energy values used by Li et al. (1995).

The FEFF 6.0.1 package has been used to calculate multiple-scattering XAFS spectra for the Al-rich $MgSiO_3$ perovskite (Rehr et al. 1992). Potentials for each type of atoms were calculated using the muffin-tin approximation, with the automatic overlap function. We chose the Hedin-Lundquist potential as exchange potential, and used a zero imaginary part in the potential (i.e., the code defaults). Cluster size and maximum path length were set to 7 Å, thus up to 177 atoms absorbing atoms were considered around the perovskite dodecahedra and up to 167 around octahedra. The number of scattering paths was limited to eight in all cases. For 7 Å clusters, and using default path filters (2 and 4% for plane and curved wave, respectively), about a 1000 paths contribute to the absorption spectra calculations. Reducing the size of the cluster below 6 Å results in a significant modification of the shape of the absorption spectra. Calculations performed using a cluster larger than 7 Å show that the spectra are not significantly improved, although the computing-time becomes unacceptable. For calculations at the Al *K*-edge, we performed two different calculations: assuming that Al is located in either the octahedral or the dodecahedral sites, for both assuming that the surrounding structure is unchanged $MgSiO_3$ perovskite. For the Si *K*-edge, the energy range of the theoretical spectra needed to be multiplied by a factor of 1.25, in order to better model the features found in the experimental spectrum. This suggests that Si^{4+} electronic properties could not be correctly modeled.

RESULTS

Mg *K*-edge XAFS

XAFS spectra at the Mg *K*-edge in various compounds (Fig. 1) confirm that the first resonance (peak C) found at low energy and related to transition from the 1s to 2p states, shifts toward higher energies as coordination number increases (Ildefonse et al. 1995). The shift is about 1.3 eV between Mg with CN = 6 (enstatite) and CN = 12 (perovskite). A shift is also observed between spectra recorded for pyrope and perovskite, despite the fact that the two compounds have a comparable Mg site, with nearest neighbor CN close to eight. In fact, the distorted dodecahedral site of $MgSiO_3$ *Pbnm* perovskite is often described by two shells such that the inner has eight O atoms and the outer has four O atoms, with mean Mg-O bond lengths of 2.20 and 2.95 Å, respectively (Ito and Matsui 1978; Ross and Hazen 1989). The energy shift of the first resonance can also be correlated with the mean Mg-O bond-length increasing from 1.92 to 2.45 Å from spinel to perovskite.

Results of multiple scattering calculations (FEFF-6) are presented in Figure 2. Cluster size and maximum path length were set to 7 Å, thus involving up to 177 atoms. Agreement is satisfactory between the experimental and calculated spectra (see vertical lines drawn in Fig. 2). In

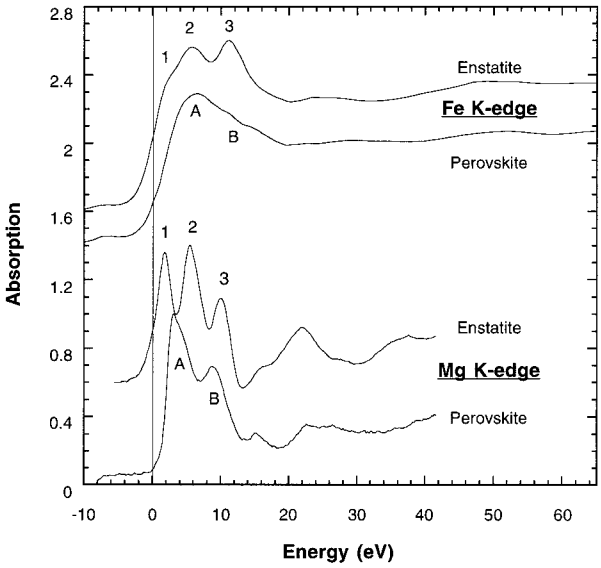

FIGURE 3. Mg and Fe *K*-edge experimental XAFS spectra for enstatite and perovskite. For both elements, the enstatite absorption edge was used to define a reference for the energy scale. Both enstatite near-edge spectra contain three main features (1, 2, 3) above the absorption edge, while only two are observed for perovskites (A,B).

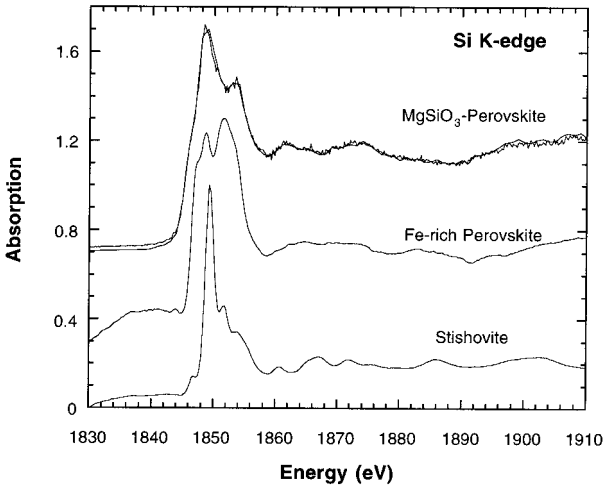

FIGURE 4. Si *K*-edge XAFS spectra of $MgSiO_3$ and $(Mg_{0.9},Fe_{0.1})SiO_3$ perovskites and stishovite. The edge peaks of the perovskite absorption spectrum is changed significantly due to partial Fe substitution for Mg in the second shell. Spectra for $MgSiO_3$ perovskite are raw data using two different energy steps for the monochromator, showing the good reproducibility of the results.

the near edge region, the calculation accurately reproduces the position of the three contributions observed in the experimental spectrum, although intensities are not identical. At higher energies, the three features are located between 1330 and 1380 eV, but their absolute energy positions are not perfectly reproduced, probably related to limitation of the code used.

X-ray absorption spectra for Fe^{2+} in $(Mg,Fe)SiO_3$ perovskite have been reported previously (Jackson et al. 1987; Farges et al. 1994). We present in Figure 3 spectra recorded at both Mg and Fe *K*-edges for the enstatite and perovskite. The spectra are better defined at the Mg than at Fe *K*-edges because of difference in lifetime of core holes. Both enstatite near-edge spectra contain three main features (1, 2, 3), consistent with the local structure around Mg^{2+} and Fe^{2+} being similar in all pyroxenes. For both elements, perovskite show an absorption edge at higher energy than for enstatite. The energy shifts between enstatite and perovskite are not identical at Mg and Fe *K*-edges, an effect that could be due to differences in cation electronic properties. Both perovskite spectra contain two main features (A,B) located close to the absorption edge. The close similarity between these perovskite spectra strongly suggests that Fe^{2+} is located in the same polyhedron as Mg^{2+} in the $MgSiO_3$ perovskite, namely the dodecahedral site. This same conclusion was derived from FEFF-6 calculations at the Fe *K*-edge (Farges 1995).

Si *K*-edge XAFS

XANES spectra were recorded at the Si *K*-edge of stishovite, and $MgSiO_3$ and $(Mg_{0.9},Fe_{0.1})SiO_3$ perovskites (Fig. 4). The stishovite spectrum is similar to that reported in Li et al. (1993) and Henderson et al. (1995). Absorption edge features are broader in the perovskites than in stishovite. In stishovite, SiO_6 octahedra have a tetragonal distortion, with four Si-O distances at 1.757 and two distances at 1.808 Å (Hill et al. 1983). Bond length variation is higher than in perovskite, which has two Si-O distances at 1.781, two at 1.796, and two at 1.799 Å (Ross and Hazen 1989). The more pronounced broadening of the perovskite spectrum thus probably comes from a higher number of possible photo-electron paths, due to the fact that none of the SiO_6 octahedral axes align along the orthorhombic *Pbnm* unit-cell edges.

The second shell around the Si absorbing element is formed by atoms located in dodecahedra. The first absorption band of the XANES part is significant affected by partial Fe substitution in the dodecahedra (Fig. 4). The spectral modification is probably mostly due to change of the atomic weight between Mg and Fe than to variation of the local structure, because X-ray diffraction showed that the perovskite cell parameters are a little affected by the (Mg,Fe) solid solution (Parise et al. 1990).

As observed for the Mg spectra in various compounds, the position of the first resonance of the Si *K*-edge shifts toward higher energies with increasing coordination numbers. The shift of about 1.2 eV between enstatite (Si, CN = 4) and perovskite (Si, CN = 6) is comparable to the shift of 1.3 eV for Mg spectra from spinel (Mg, CN = 4) and enstatite (Mg, CN = 6). There is a similar shift of about 1.9 eV between quartz and stishovite spectra. Note that the perovskite spectrum might contain a small amount of glass due to the onset of back-transformation

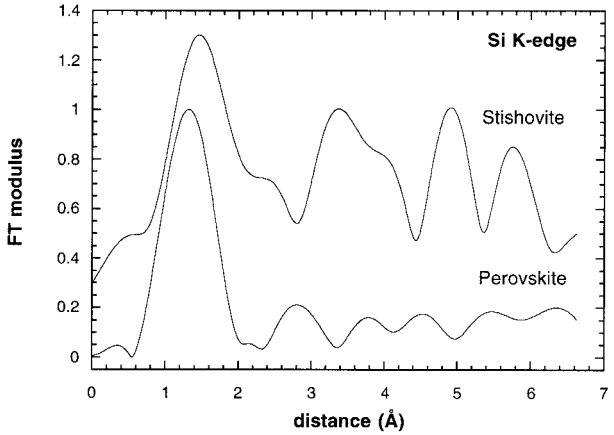

FIGURE 5. K^3-weighted Fourier transform of the normalized EXAFS oscillations of stishovite and $MgSiO_3$ perovskite. The dominant peaks observed around 1.7 Å (not corrected for phase shifts) correspond to the Si-O bonds in SiO_6 octahedra. The FT spectra of stishovite show contributions for much distant neighbor shells than perovskite, suggesting a more symmetrical medium range order.

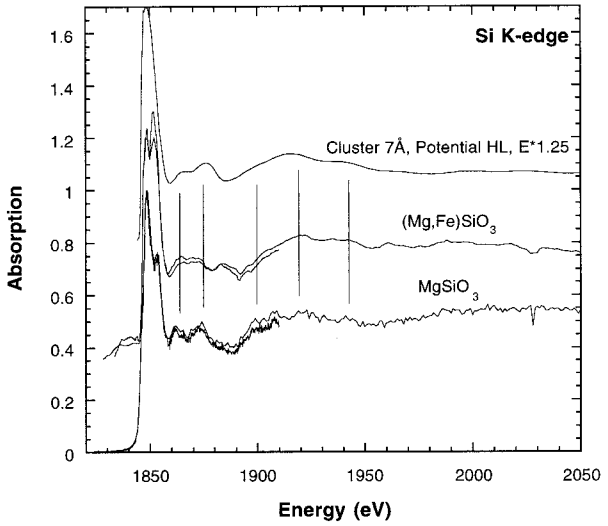

FIGURE 6. Si *K*-edge experimental XAFS spectra and multiple scattering calculation (FEFF-6) for $MgSiO_3$ perovskite. Cluster size and maximum path length were set to 7 Å, thus containing up to 167 atoms. Vertical lines correlate equivalent features.

of this metastable high-pressure polymorph (see Andrault et al. 1996).

The k^3-weighted Fourier transforms (FT) of the normalized EXAFS oscillations (see Teo 1986; Andrault et al. 1996) of stishovite and $MgSiO_3$ perovskite (Fig. 5) both have first contributions of the Si-O bonds in SiO_6 octahedra around 1.7 Å. The FT spectra of stishovite show contributions at much higher distances than perovskite, a sign of more symmetric local order. This was already clear from the XANES spectra (Fig. 4) that show much stronger oscillations for stishovite.

Multiple scattering calculations were performed for the Si *K*-edge in the silicate perovskite, using the neighbor shells around the octahedrally coordinated Si of Ross and Hazen (1989). Cluster size and maximum path length were set to 7 Å, thus involving up to 167 atoms. All calculated features are found at lower energies than for experimental measurements. In Figure 6, we thus scaled the energy axis of theoretical spectra by a factor of 1.25, to better match the perovskite experimental spectra (see vertical lines between experimental and calculated spectrum). This difference might be related to the high Si^{4+} charge that affects the exchange potential used in the FEFF-6 calculation. As seen for the Mg *K*-edge, a large part of the absorption spectra is fairly well reproduced. The five characteristic features located between 1860 and 1950 eV are present, but absorption-edge is not well calculated. Other types of theoretical calculations could be used to improve agreement with experimental spectrum, but are not central to this paper.

Al *K*-edge XAFS

XAFS Al *K*-edge spectra for various Al-local structures are presented in Figure 7. These structures consist of Al located in tetrahedra (albite), regular octahedra (pyrope), distorted octahedra (corundum), and the unknown site in $(MgSi)_{0.85}Al_{0.3}O_3$ perovskite. As described above for the Mg and Si *K*-edges, the energy position of the main Al *K*-edge peak (peak C) increases with increasing Al coordination number. The lower energy part of the perovskite spectrum appears quite similar to that of corundum, but experimental features are all shifted toward higher

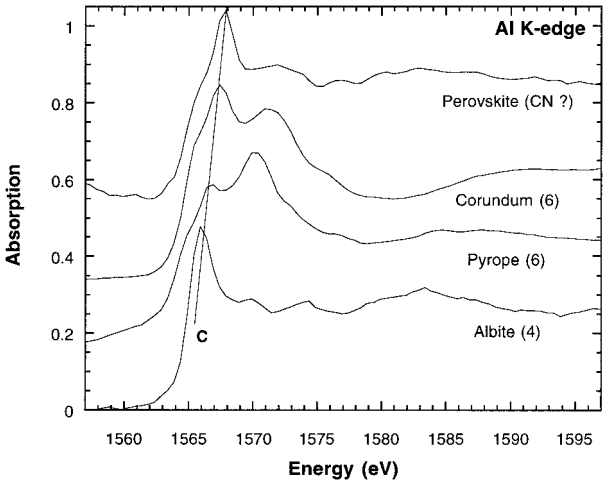

FIGURE 7. Al *K*-edge XAFS spectra of albite (Al, CN = 4), pyrope (Al, CN = 6 regular), corundum (Al, CN = 6 distorted), and Al-rich perovskite (Al, CN to be determined). Energy positions of the main Al *K*-edge peak (C) increase with increasing Al coordination number. The lower energy part of the perovskite spectrum appears quite similar to that of corundum, but experimental features are all shifted toward higher energies.

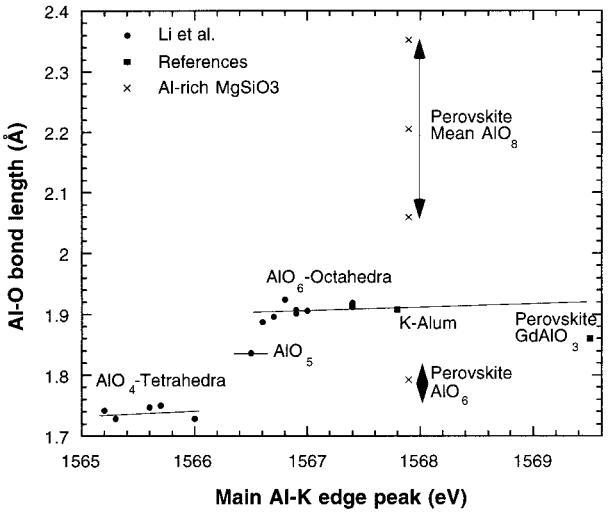

FIGURE 8. Correlation between peak C energy position and Al-O bond length in various compounds. Partially derived from Li et al. (1995). Other references are Ildefonse et al. (1997) and Landron et al. (1991). The position of peak C in perovskite (1567.9 eV) is not compatible with Al in either octahedral (AlO_6) or dodecahedral (AlO_8) sites. Instead of 1.792 or [2.02–2.42] Å that could correspond to possible Al-O bond length in the Al-rich $MgSiO_3$ perovskite (see text), a mean Al-O bond length of 1.91 Å is suggested for an energy-peak located at 1567.9 eV.

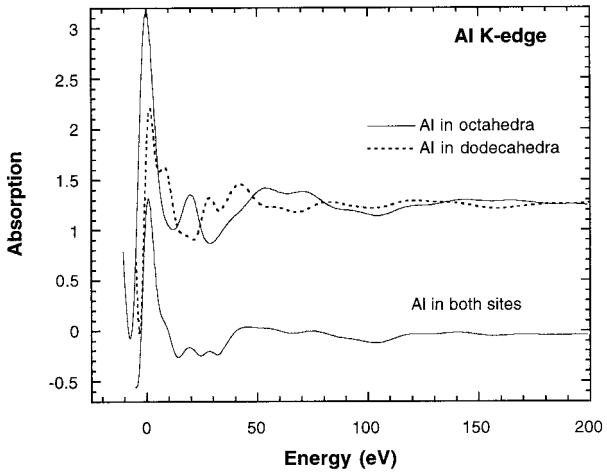

FIGURE 9. Al *K*-edge multiple scattering calculation (FEFF-6) for $MgSiO_3$ perovskite. The two upper curves correspond to calculations made for Al located in either octahedra or dodecahedra. None of these calculations adequately represents the experimental XAFS spectrum. The bottom curve is a simple average of the upper spectra, corresponding to equi-partition of Al between the two types of polyhedra.

energies. The maximum of the perovskite spectrum is also found at higher energy than the peak C of the pyrope spectrum, suggesting that the Al atomic site in perovskite has a coordination number larger than six. However, XANES features are also modified by variation in parameters other than coordination number, such as mean Al-O bond length or distortion of the local structure, as suggested by the shift in energy between pyrope and corundum.

Li et al. (1995) followed the evolution of the peak C in many different compounds. They proposed a correlation between peak C energy positions and Al-O bond lengths. Figure 8 is derived from their study, and includes data from other previous reports and the present results. We re-calibrated the energy scale of previous studies, to compare all the results in the same diagram (see experimental section). We have added results related to the Al in the regular octahedral site of potassium-alum [$KAl(SO_4)_2 \cdot (H_2O)_{12}$, 1567.8 eV, Ildefonse et al. 1997], in distorted octahedra of $GdAlO_3$ rhombohedral perovskite (Landron et al. 1991), and in Al-rich $MgSiO_3$ perovskite (this study). The potassium-alum data point appears close to the trend drawn in Figure 8, suggesting a slight increase of the peak C energy with increasing bond length. This is not the case for $GdAlO_3$ perovskite, where peak C is found at a much higher energy, for a smaller Al-O bond length than usually found for AlO_6 octahedra. This information suggests that deviation from usual Al-O octahedral bond lengths (between 1.89 and 1.92 Å) significantly affects the energy position of the peak C. The variation of the bond length could induce modification of local charge density, which would affect the exchange potential, and thus the energy position in the absorption spectra.

For the Al-rich perovskite, peak C occurs at about 1567.9 eV. If we assume that the perovskite sites are not distorted by the Al-substitution, the Al-O bond distances expected for the octahedral or dodecahedral sites [1.792 or (2.02–2.42) Å, respectively] are not consistent with the energy trend in Figure 8 for the Al-octahedra. Instead of 1.792 or 2.205 Å, the energy trend would suggest an Al-O bond length around 1.91 Å for an energy peak located at 1567.9 eV, as it is observed for potassium-alum (1567.8 eV). Such a large variation in bond length (from 1.91 to 1.792 Å or from 1.91 to 2.205 Å) should produce a significant modification of the position of the peak C, as illustrated by the discontinuity between the trends for AlO_4 [Peak C between 1565.2 and 1566 eV for d(Al-O) of around 1.74 Å] and AlO_6 polyhedra (between 1566.6 and 1568 eV for around 1.9 Å). Thus, our results cannot be explained assuming that Al is located in only one of the two sites. Either the perovskite Al site is very distorted in comparison with those of $MgSiO_3$, or Al is located on both of the sites. In fact, the latter value of 1.91 Å is much closer to the mean bond length between the two polyhedra, suggesting that Al is distributed over both of the perovskite polyhedra.

The multiple scattering calculations were performed for each hypothesis assuming that Al is located in the octahedral or dodecahedral site (Fig. 9). Calculated spectra are found to be comparable to those of Mg and Si *K*-edge in their respective sites in the perovskite (Figs. 2

and 6). None of these spectra correctly reproduced the experimental features at the Al *K*-edge. Similarly, the experimental Al *K*-edge spectrum is not comparable to those recorded for Si-octahedral and Mg-dodecahedral sites. Thus, we are left with two possibilities. The first is that Al is located in a highly distorted site. This, however, should produce a significant modification of the unit-cell parameters (*a*,*b*,*c*) of the perovskite. It is not compatible with the reported X-ray diffraction pattern of $Mg_3Al_2Si_3O_{12}$ perovskite, which is found to be very close to that of $MgSiO_3$ composition perovskite (Irifune et al. 1992; see Table 1).

The second hypothesis is that Al resides equally in both octahedral and dodecahedral sites. We calculated an average spectrum using this hypothesis (Fig. 9). The most important feature is a significant reduction of the EXAFS modulation intensities. This low definition of the EXAFS modulation is also observed in experimental spectra, although the average spectrum does not match the experimental data satisfactorily. However, it would have been very surprising to reproduce quantitatively the experimental spectrum with such a simple averaging. Indeed, slight modification of the energy scale between octahedral and dodecahedral Al-spectra would produce a large variation in the shape of the average spectra. This energy scale modification between sixfold and 12-fold coordination number is likely to happen, as is evidenced in Figure 1 for the Mg absorption edge.

Discussion

Ionic radii

Discussion of the location of Al^{3+} in Al-rich $MgSiO_3$ perovskite is related to possible structure adaptation in terms of charge balances and ionic radii. The effective ionic radius of Al^{3+} lies between those of Si^{4+} and Mg^{2+} (Shannon and Prewitt 1969), which should introduce significant modification in the local structure of the compact perovskite. Kudoh et al. (1992) used the following expression to describe changes of ionic radius (r) as a function of the cation valence (Z) and coordination number (n) in perovskites:

$$r = \mathrm{a} + \mathrm{b} \log(Z/n) \quad (1)$$

For each cation, a remarkable correlation was observed, for r and Z/n values of various atomic site, and using a and b as empirical constants. For octahedrally coordinated Si^{4+} (Z/n value of 4/6), the effective radius is 0.40 Å. Similarly, radii of 0.86 and 1.04 Å are found for Mg^{2+}, when the dodecahedral CN is taken as 8 or 12 (Z/n = 2/8 or 2/12), respectively. For Al^{3+} (where a = 0.28 Å and b = −0.85 Å, Kudoh et al 1992), the expected radii are 0.54 Å (Z/n = 3/6) in octahedra, and 0.64 or 0.79 Å (Z/n = 3/8 or 3/12) in dodecahedra. These Al ionic radii differ significantly from those of Si^{4+} and Mg^{2+} in each polyhedron, differences that seems to contradict the ready substitution of Al in mantle perovskite.

Kudoh et al. (1992) proposed that the Z/n values found for the SiO_6 and MgO_8 or MgO_{12} sites correspond to the effective bond strengths in respective octahedra and dodecahedra of the $MgSiO_3$-type perovskite. They claimed that these Z/n values should be used to evaluate ionic radii of other elements that would locate in this same structure. On this basis, one would expect Al^{3+} radii of 0.43 Å for location in the SiO_6-type octahedra (Z/n = 4/6) and 0.79 and 0.94 Å for Mg-type dodecahedra (Z/n = 2/8 or 2/12). These new calculated Al^{3+} radii are found to be close to those of Si^{4+} (0.40 Å) and Mg^{2+} (0.86 or 1.04 Å) in their respective polyhedra, thus giving a clue to the important Al-substitution in $MgSiO_3$ perovskite. However, since Al is trivalent, it is questionable whether the effective bond strength of 4/6 instead of 3/6 should be used to evaluate Al^{3+} radius in the octahedra (and 2/8 instead of 3/8 for dodecahedra).

Electronic charges in Al-rich $MgSiO_3$

We propose that charge transfer possibly occurs between octahedra and dodecahedra in the perovskite structure through the O positioning (electric balance is only needed for the unit cell, polyhedra can be charged). In an hypothetical cubic $MgSiO_3$ perovskite, 12 O atoms would contribute to the global dodecahedron electronic charge, equivalent to twice the O bonds for the Mg^{2+} cation than for Si^{4+} in the octahedral site. In a distorted dodecahedron for orthorhombic $MgSiO_3$ perovskite, four O atoms are found far from the central Mg^{2+}, between 2.84 and 3.12 Å in comparison with the mean value of 2.20 Å for the eight closer O atoms. It is possible that these four distant O atoms will not contribute to the dodecahedron charge. We suggest that the orthorhombic distortion produces a modification of the charge balance between octahedra and dodecahedra. Thus, there would be fewer negative charges contributing to dodecahedra (more to octahedra) that would also reply to the charge differences between Mg^{2+} and Si^{4+}.

If such local charge modification is possible, the Al^{3+} substitution in the $MgSiO_3$ perovskite is easier to understand. First, Al^{3+} substitution reduces charges of octahedra (Al^{3+} substitutes for Si^{4+}) and increases charges in dodecahedra (Al^{3+} substitutes for Mg^{2+}), making local neutrality easier to attain. Also, it is possible that slight modification of the dodecahedral distortion can help to resolve the charge modifications imposed by the Al-substitution in both polyhedra. Thus, for a coupled-substitution in both sites of Al-rich $MgSiO_3$ perovskite, the effective charges of AlO_6 octahedra and AlO_8 dodecahedra could simply be similar to those found for SiO_6 or MgO_8.

These considerations suggest that the polyhedral effective charge is a more important parameter than the cation charge itself. This could better explain the proposition of Kudoh et al. (1992) to calculate the atomic radii using the polyhedral bond strength (Z/n where Z would better relate to polyhedral effective charge) of the global structure instead of that calculated for each particular ions. This type of easy electronic balance between sites is only conceivable in an equilibrated structure, where no charged vacancies are needed to maintain electroneutral-

ity, again suggesting that Al-substitution occurs on both of the perovskite sites.

Conclusion

Our main argument for Al being located in both of the perovskite coordination sites reside in the Al *K*-edge spectrum being largely different from those recorded at Si and Mg *K*-edges in the same structure. As mentioned above, this evidences either a large distortion of one of the coordination sites (incompatible with X-ray results), or a coupled substitution on both Mg and Si sites. In a coupled substitution model, it is also possible that Al induces a slight distortion of each polyhedron, but this distortion can remain a local effect as soon as the AlO_{12} and AlO_6 sites are adjacent. The O lattice would probably at any rate sustain only reduce local modification.

It is also possible that for a limited proportion of the Al content, substitution occurs through a second mechanism. For example, a certain preference of Al for one of the two polyhedral sites could induce an atomic exchange, such as the one proposed in the introduction between dodecahedral-Mg and octahedral-Al. The perovskite crystal chemistry would then slightly evolve from $(Mg_{0.85}Al_{0.15})(Al_{0.15}Si_{0.85})O_3$ toward $(Mg_{0.7}Al_{0.3})(Mg_{0.15}Si_{0.85})O_3$ end-member perovskite. Nevertheless, our results evidence that such an effect is to remain second order.

Acknowledgments

We thank F. Farges, P. Ildefonse, and P. Lagarde for their help and useful comments related to light element XAFS spectroscopy. The synthesis experiments were performed at the Stony Brook High Pressure Laboratory, which is jointly supported by SUNY Stony Brook and the NSF Science and Technology Center for High Pressure Research (EAR 89-20239). Reviews and comments given by A. Hofmeister, J.P. Poirier, F. Seifert, and by C.M.B. Henderson and an anonymous referee are gratefully appreciated. CNRS-INSU-DBT IPGP contribution no. 1547.

References cited

Andrault, D. and Poirier, J.P. (1991). Evolution of the distortion of Perovskites under pressure: an EXAFS study of $BaZrO_3$, $SrZrO_3$, and $CaGeO_3$. Physics and Chemistry of Minerals, 18, 91–105.

Andrault, D., Itié, J.P., and Farges, F. (1996) High-temperature structural study of germanate perovskites and pyroxenoids. American Mineralogist, 81, 822–832.

Cabaret, D., Sainctavit, P., Ildefonse, P., and Flank, A.-M. (1996) Full multiple-scattering calculations on silicates and oxides at the Al K edge, Journal of Physics: Condensed Matter, 8, 391–3704.

Farges, F. (1995) The site of Fe in Fe-bearing $MgSiO_3$ enstatite and perovskite. A theoretical-, X-ray multiple-scattering study at Fe K-edge. Physics and Chemistry of Minerals, 22, 318–322.

Farges, F., Guyot, F., Andrault, D., and Wang, Y. (1994) Local structure around Fe in $Mg_{0.9}Fe_{0.1}SiO_3$ perovskite: An X-ray absorption spectroscopy study at Fe-K edge. European Journal of Mineralogy, 6, 303–312.

Fisher, M., Bonello, B., Itie, J.P., Polian, A., Fontaine, A., and Dartyge, E. (1990) X-ray absorption spectroscopy on strontium titanate under high pressure. Physical Review B, 42, 8994.

Henderson, C.M.B., Cressey, G., and Redfern, S.A.T. (1995) Geological applications of synchrotron radiation. Radiation Physics Chemistry, 4, 459–481.

Hill, R.J., Newton, M.D., and Gibbs, G.V. (1983) A crystal chemical study of stishovite. Journal of Solid State Chemistry, 47, 185–200.

Irifune, T., Adachi, Y., Fujino, K., Ohtani, E., Yoneda, A., and Sawamoto, H. (1992) A performance test for WC anvils for multianvil apparatus and phase transformation in some aluminous minerals up to 28 GPa. In Y. Syono and M.H. Manghnani, Eds., High-pressure research: Application to Earth and planetary sciences, p. 43–50. American Geophysical Union, Washington, D.C.,

Ildefonse, P., Calas, G., Flank, A.-M., and Lagarde, P. (1995) Low Z elements (Mg, Al, and Si) K-edge X-ray absorption spectroscopy in minerals and disordered systems. Nuclear Instruments and Methods in Physics Research, B97, 172–175.

Ildefonse, P., Cabaret, D., Sainctavit, P., Calas, G., Flank, A.-M., and Lagarde, P. (1998) Aluminum X-ray absorption near edge structure in model compounds and Earth's surface minerals, Physics and Chemistry of Minerals, 25, 112–121.

Ito, E. and Matsui, Y. (1978) Synthesis and crystal-chemical characterization of $MgSiO_3$ perovskite. Earth and Planetary Science Letters, 38, 443–450.

Jackson, W.E., Knittle, E., Brown, G.E., and Jeanloz, R. (1987) Partitioning of Fe within high-pressure silicate perovskite: evidence for unusual geochemistry in the lower mantle. Geophysical Research Letters, 14, 224–226.

Kesson, S.E., Fitz Gerald, J.D., Shelley, J.M., and Withers, R.L. (1995) Phase relations, structure and crystal chemistry of some aluminous silicate perovskites. Earth and Planetary Science Letters, 134, 187–201.

Kudoh, Y., Prewitt, C.T., Finger, L.W., and Ito, E. (1992) Ionic radius-bond strength systematics, ionic compressibilities, and an application to $(Mg,Fe)SiO_3$ perovskites. In Y. Syono and M.H. Manghnani, Eds., High-pressure research: Application to Earth and planetary sciences, p. 215–218. American Geophysical Union, Washington, D.C.

Landron, C., Badets, M.C., Douy, A., Coutures, J., Coutures, J.P., Daniel, P., and Flank, A.-M. (1991) Evidence of tetrahedral and octahedral aluminum coordination in rare-Earth aluminates. Physica Status Solidi, b, 167, 429–440.

Liu, L.G. (1974) Silicate perovskite from phase transformations of pyrope-garnet at high-pressure and temperature. Geophysical Research Letters, 1, 277–288.

Li, D., Bancroft, G.M., Kasrai, M., Fleet, M.E., Feng, X.H., Tan, K.H., and Yang, B.X. (1993) High resolution Si K- and $L_{2,3}$-edge XANES of α quartz and stishovite. Solid State Communications, 87, 613–617.

Li, D., Bancroft, G.M., Kasrai, M., Fleet, M.E., Secco, R.A., Feng, X.H., Tan, K.H., and Yang, B.X. (1994) X-ray absorption spectroscopy of silicon dioxide (SiO_2) polymorphs: The structural characterization of opal. American Mineralogist, 79, 622–632.

Li, D., Bancroft, G.M., Fleet, M.E., Feng, X.H., and Pan, Y. (1995) Al *K*-edge XANES spectra of aluminosilicate minerals. American Mineralogist, 80, 432–440.

Natoli, C.R. and Benfatto, M. (1986) A unifying scheme of interpretation of X-ray absorption spectra based on multiple scattering theory. Journal de Physique, Colloque C8, 47, 11–23.

Parise, J.B., Wang, Y., Yeganeh-Haeri, A., Cox, D.E., and Fei, Y. (1990) Crystal structure and thermal expansion of $(Mg,Fe)SiO_3$ perovskite. Geophysical Research Letters, 17, 2089–2092.

Rehr, J.J., Zabinsky, Z.I., and Alberts, R.C. (1992) High-order multiple scattering calculations of x-ray-absorption fine structure. Physical Review Letters, 69, 3397–4000.

Ross, N.L. and Hazen, R.M. (1989) Single crystal X-ray diffraction study of $MgSiO_3$ perovskite from 77 to 400 K. Physics and Chemistry of Minerals, 16, 415–420.

Shannon, R.D. and Prewitt, C.T. (1969) Effective ionic radii in oxides and fluorides. Acta Crystallographia, B25, 925–946.

Sharp, T., Wu, Z., Seifert, F., Poe, B., Doerr, M., and Paris, E. (1996) Distinction between six- and fourfold coordinated silicon in SiO_2 polymorphs via electron loss near edge structure (ELNES) spectroscopy. Physics and Chemistry of Minerals, 23, 17–24.

Teo, B.K. (1986) EXAFS: Basic principles and data analysis. Springer, Berlin Heidelberg New York.

Téqui, C., Robie, R.A., Hemingway, B.S., Neuville, D.R., and Richet, P. (1991) Melting and thermodynamic properties of pyrope ($Mg_3Al_2Si_3O_{12}$). Geochimica Cosmochimica Acta., 55, 1005–1011.

Thomson, K.T., Wentzcovitch, R.M., and Bukowinski, M.S. (1996) Polymorphs of alumina predicted by first principles: putting pressure on the ruby pressure scale, Science, 274, 1880–1882.

Wang, Y., Weidner, D.J., and Guyot, F. (1996) Thermal equation of state of $CaSiO_3$ perovskite. Journal of Geophysical Research, 101, 661–672.
Wu, Z., Seifert, F., Poe, B., and Sharp, T. (1996) Multiple scattering calculations for SiO_2 polymorphs: A comparison to ELNES and XANES spectra. Journal of Physics: Condensed Matter, 8, 3323–3336.
Yusa, H., Yagi, T., and Shimobayashi, N. (1995) A new unquenchable high-pressure polymorph of $Ca_3Al_2Si_3O_{12}$. Physics of the Earth and Planetary Interiors, 92, 25–31.

Manuscript received September 22, 1997
Manuscript accepted April 30, 1998
Paper handled by Gilberto Artioli